The Impact of Organic Additives on Copper Trench Microstructure

James B. Marro,[a,b,z] Chukwudi A. Okoro,[c] Yaw S. Obeng,[c,*] and Kathleen C. Richardson[a,b]

[a]*Glass Processing and Characterization Laboratory, College of Optics and Photonics, CREOL - University of Central Florida, Orlando, Florida 32816, USA*
[b]*School of Material Science & Engineering, Clemson University, COMSET, Clemson, South Carolina 29634, USA*
[c]*Engineering Physics Division, National Institute of Standards and Technology (NIST), Gaithersburg, Maryland 20899, USA*

Organic additives are typically used in the pulse electrodeposition of copper (Cu) to prevent void formation during the filling of high aspect ratio features. In this work, the role of bath chemistry as modified by organic additives was investigated for its effects on Cu trench microstructure. Polyethylene glycol (PEG), bis(3-sulfopropyl) disulfide (SPS), and Janus green b (JGB) concentrations were varied in the Cu electrodeposition bath. Results indicated a correlation between the JGB/SPS ratio and the surface roughness and residual stresses in the Cu. Electron backscattering diffraction (EBSD) and transmission Kikuchi diffraction (TKD) were used to study the cross-sectional microstructure in the trenches. Finer grain morphologies appeared in trenches filled with organic additives as compared to additive-free structures. Cu trench (111) texture also decreased with increasing organic additive concentrations due to more pronounced influence of sidewall seed layers on trench features. Twin density in the microstructure closely tracked calculated stresses in the Cu trenches. A comprehensive microstructural analysis was conducted in this study, on an area of focus that has garnered little attention from the literature, yet can have a major impact on microelectronic reliability.

Manuscript submitted April 21, 2017; revised manuscript received May 15, 2017. Published June 28, 2017. This was Paper 1099 presented at the San Diego, California, Meeting of the Society, May 29- June 2, 2016.

Since it replaced aluminum in the 1980's, copper (Cu) has become the primary material for microelectronic interconnects for its low electrical resistance.[1] However, copper's high coefficient of thermal expansion (CTE) compared to the surrounding materials, such as silicon, in these multi-material systems can result in many thermo-mechanical stresses/defects.[2–4] Preferentially oriented Cu microstructures with large twin densities have been shown to improve reliability of interconnects by increasing thermal stability, mechanical strength, and electromigration resistance.[5–9] While desirable highly textured Cu has been achieved in low aspect ratio features,[10–12] only randomly oriented microstructures have been found in high aspect ratio vias.[2,13,14]

Pulse electrodeposition (PED) is typically used to fill trenches and other advanced features in microelectronics. Sub-conformal or conformal filling from the sidewalls of these features may trap air and produce voids, which degrade the signal integrity of the interconnects.[2,15] To achieve defect-free features, a technique known as bottom-up filling (super-filling) is utilized, in which modification of the bath's chemistry has been shown to reduce such defect formation.[16–18] Three main types of organic additives used in the electrodeposition bath are accelerators, suppressors, and levelers. Accelerators, such as bis(3-sulfopropyl) disulfide (SPS), perform as catalysts to the Cu deposition at the base of the features. Suppressors and levelers function as inhibitors of the Cu deposition. Suppressors, such as, polyethylene glycol (PEG), prevent growth on the sidewalls of the features, while the levelers, for example, Janus green-b (JGB) prevent the formation of overfill bumps. The specifics of the chemical mechanisms associated with the favorable role of these additives in PED baths are still relatively unknown.[19] That said, the curvature-enhanced accelerator (CEAC) model proposed by Moffat et al. is widely accepted as the model for bottom-up filling of features with organic additive-containing baths.[20] This model suggests that the accelerator and suppressor compete for sites on the copper surface and the accelerator coverage is dictated by the surface's curvature.[21]

While organic additives have been studied extensively as a mechanism for reducing filling defects, their direct impact on the resulting, post-deposition microstructure is still widely unknown. Finer grains have been found in Cu deposited with organic additives.[11,22] An increase in cathodic over-potential results in lower activation energy for nucleation and smaller Cu grains. Several studies have observed this when inhibitors are used in the deposition.[23,24] Furthermore, Neuner et al. and Manu et al. found evidence that organic additives may slightly affect the crystallographic orientation of Cu.[11,25] However, these studies are limited to the surface microstructure of the Cu and have not directly examined the role of additives on sub-surface microstructure.

This paper summaries the findings from a comprehensive and systematic study that examined the effects of organic additives on the extrinsic properties (surface roughness, residual stress, grain size, orientation, and twins) of Cu deposited into low-aspect trenches.[26] Here, we aim to further elucidate, and confirm, the role of the additives in copper electroplating into patterned structures. Furthermore, we assess the role of organic additives in the creation of defects in the Cu microstructural evolution, such as pinning grain boundary movement, and interfering with the atomic arrangements during the deposition, resulting in changes in crystallographic orientation.

Experimental

Pulsed electrodeposition of Cu films.—Patterned substrates (20 mm × 20 mm) with low aspect ratio trenches, ranging from 0.005 to 2.78, were used in the work reported in this paper (SKW-6,[d] SKW Associates Inc. Santa Clara, CA, USA). Figure 1 shows a cross-sectional illustration and SEM image of the multi-material substrates used in this study. All trenches had a depth of 500 nm with varying widths (180 nm to 100,000 nm). Copper was electrodeposited onto the seeded copper substrates using a two electrode pulse electrodeposition (PED) setup with a 99.9999% pure Cu anode. A 50 Hz square waveform with a duty cycle of 0.1 was chosen based on findings from a previous study,[27] as these conditions produced a Cu film with high twin densities, large grain sizes, low biaxial residual stresses, and highly preferential (111) orientation. These microstructural characteristics are desirable, and believed to be essential in reducing thermo-mechanical stresses in

*Electrochemical Society Member.
[z]E-mail: jmarro@g.clemson.edu

[d]Certain commercial equipment, instruments, or materials are identified in this report in order to specify the experimental procedure adequately. Such identification is not intended to imply recommendation or endorsement by the National Institute of Standards and Technology, nor is it intended to imply that the materials or equipment identified are necessarily the best available for the purpose.

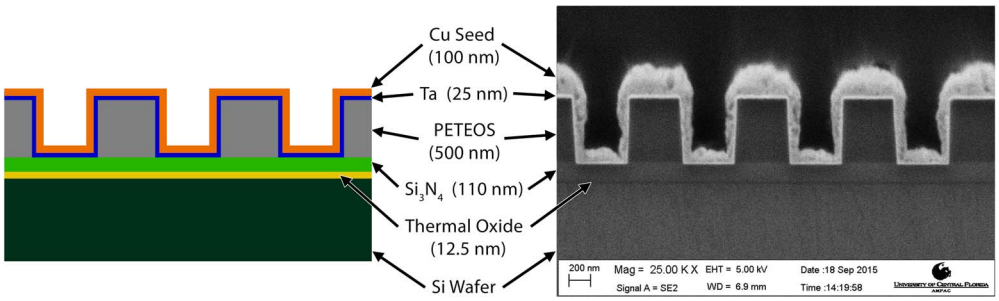

Figure 1. The cross-sectional illustration (left) and scanning electron micrograph (right) of the SKW-6 test wafer dies used for deposition.

multi-material systems such as microelectronic interconnects without degrading electrical properties of the material.[6,7,9,28,29]

The baseline inorganic constituents in the electrodeposition bath were maintained at 200 g/L of copper sulfate pentahydrate ($CuSO_4.5H_2O$), 50 g/L of ACS grade sulfuric acid (H_2SO_4), and 50 mg/L of ACS grade hydrochloric acid (HCl). Organic additives were introduced into the bath at varying concentrations as summarized in Table I. Films resulting from additive-containing depositions were compared with Cu deposited from baths without organic additives.

Prior to deposition, the baths were degassed for 30 minutes nitrogen from (99.9999% N_2, Air Liquide). Depositions were performed under a N_2 blanket, at room temperature and with a 200 rpm bath stir rate. The as-deposited samples were stabilized by annealing at 150°C for 1 hour in a forming gas atmosphere (4% H_2/96% N_2).[30,31]

Roughness and residual stress measurements.—Following electrodeposition of the Cu onto the patterned substrates and annealing, the surface roughness (RMS) and stresses were evaluated with a non-contact white light interferometer (Zygo NewView 8100). RMS roughnesses were recorded on non-patterned areas of the samples (~0.4 × 0.4 mm), while stress approximations were made using the wafer curvature technique. The radius of curvature was measured for each sample before and after Cu deposition and implemented into a modified Stoney equation[32] to approximate the biaxial residual stress from sample to sample for these complex patterned Cu samples. The equation is shown below:

$$\sigma = \left(\frac{1}{R} - \frac{1}{R_0}\right) t_f^{-1} \qquad [1]$$

where σ is the biaxial residual stress in the copper, R_0 and R are the radius of curvatures of the sample before and after deposition, respectively, and t_f is the thickness of the deposited Cu. Due to the geometry of the substrate, only relative stress measurements could be obtained from Equation 1 by eliminating the substrate contributions from the Stoney equation. Equation 1 assumes the pre-deposited samples are stress-free and the Cu thickness is uniform across the sample.

Table I. The combination of organic additive concentrations used to deposit the copper trenches for the PED deposition conditions shown.

	Organic Additives (mg/L)			
PED Condition #	PEG	SPS	JGB	JGB/SPS Ratio
1	0	0	0	N/A
2	200	5	0	0
3	200	50	10	0.2
4	200	20	10	0.5
5	200	5	5	1
6	200	5	10	2
7	200	5	50	10
8	200	5	100	20
9	100	5	10	2
10	500	5	10	2
11	500	5	100	20

Microstructural evaluation: EBSD and XRD.—Samples were prepared for cross-sectional microstructure analysis using focused ion beam milling (FIB) at North Carolina State University's Analytical Instrumentation Facility (AIF) in Raleigh, NC, USA. A FEI Quanta 3D FEG dual beam SEM/FIB was used to mill a cross-section of the 500 nm wide trenches and liftout a <100 nm thick cross-section of the 250 nm wide trenches for electron backscattering diffraction (EBSD) and transmission Kikuchi diffraction (TKD) analysis, respectively. Unlike traditional EBSD, TKD utilizes the transmission of electrons through a thinned sample to map its grain structure. TKD was necessary on the smaller trenches due to its higher spatial resolution (~10 nm compared to ~100 nm for traditional EBSD[33]). The Cu trench cross-sections were mapped to measure grain size, orientations, and degree of twinning. Efforts were made to minimize the impact of sample charging during sample mapping.

X-Ray Diffraction was conducted on the samples using a Panalytical X'Pert^3 MRD system with a Cu alpha source (Λ = 1.54056 Å wavelength) at the University of Central Florida's Material Characterization Facility (MCF) in Orlando, FL, USA. The instrument was used to confirm the orientation variations on a macroscopic scale. The degree of preferential orientation in the Cu was quantified by calculating the texture coefficient (TC):

$$TC = \frac{I_{hkl}/I^0_{hkl}}{(1/n)\sum I_{hkl}/I^0_{hkl}} \qquad [2]$$

where I_{hkl} is the intensity of crystallographic peak of interest, I^0_{hkl} is the corresponding intensity of a randomly oriented Cu specimen, and n is the total number of Cu peaks in the diffraction pattern.

Results and Discussion

Roughness and residual stress of the Cu.—Variations in surface RMS roughness and relative biaxial stress due to the organic additive bath concentrations are shown in Figures 2a and 2b respectively. Shown for comparison are additive-free samples (0 mg/L) deposited under identical preparation conditions. PEG concentration in the electrodeposition bath appeared to have little effect on both material characteristics. Although it is generally thought from the literature that the accelerator (SPS) and suppressor (PEG) competition drives changes in advanced geometry filling profiles,[21] in this study, the leveler (JGB) and accelerator (SPS) appear to have the major impacts on the Cu properties. Increasing the leveler to accelerator (i.e., JGB/SPS) ratio in the bath resulted in both a decrease in surface roughness and biaxial stress, as evident from Figures 2a and 2b.

Trenches were cross-sectioned to evaluate resulting trench microstructure by assessing the grain size, defect content, and how it related to the bath chemistry used. It was found from Figure 2c that an increase in the JGB/SPS ratio correlated with an increase in void content within the Cu trenches. Figure 3 shows the large volume fraction of voids observed. The voids located in the center of the trenches

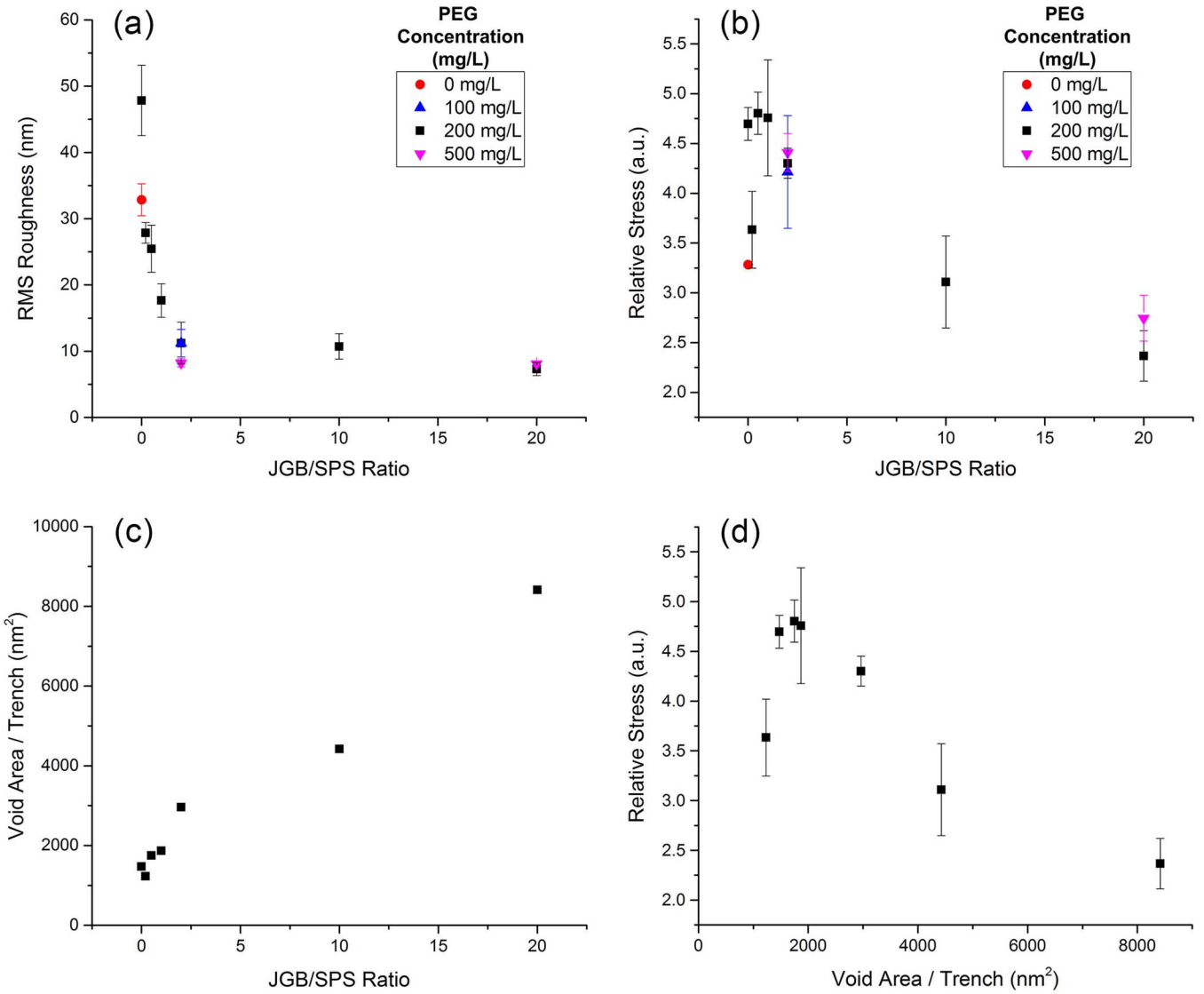

Figure 2. The surface RMS roughness (a), relative biaxial stress (b), and void area (c) with variations in JGB/SPS ratio and PEG concentration. The relationship between relative stress and void area is also shown (d). Figures (c) and (d) contain data for depositions using PEG concentrations of 200 mg/L and different SPS and JGB values. Each integer for the relative stress represents a change of approximately 10 to 15 MPa.

are believed to form as the rough sidewall surfaces of the Cu collided during the deposition. Bottom-up filling of the trenches was stunted by higher leveler (JGB) and lower accelerator (SPS) concentrations as seen in the 2.78 aspect ratio trenches. Furthermore, it can be seen that trenches deposited with a JGB/SPS ratio above 2 contained elongated voids at the grain boundaries. These voids are suspected to have formed as part of the material's 'coping mechanism' to reduce stresses during the deposition. Specifically, voids form to alleviate stress concentrations from developing at triple junctions and grain boundaries. This mechanism can be inferred from the proportional correlation between void area and stress shown in Figure 2d. The initial rise in biaxial stress, shown in Figures 2b and 2d, is not fully understood. However, it is hypothesized that there is a competition between the increased lattice strain caused by the impurities[34] and the stress relief from void formation.[35] Once a critical void area is observed in the Cu (~2000 nm^2 per trench in this study), there is a major reduction in stress.

Trench grain morphology.—Since the JGB/SPS concentration ratio during deposition appeared to have a significant impact on the material stress and void properties observed in the Cu trenches, microstructural analysis was performed only on four PED conditions (#1,4,6, and 8 from Table I) as these samples were expected to give further insight into the physical property changes observed in Roughness and residual stress of the Cu section. The microstructures of the 250 nm and 500 nm wide trenches deposited without organic additives (0/0/0) and with three selected JGB/SPS ratios (0.5, 2, 20) were observed using EBSD and TKD to assess the grain morphology in the trenches. The average grain sizes and percent area of the large grains (>200 nm) occupied within the trench is shown in Table II for each deposition condition.

It was observed that due to the large grain size distribution in the trench cross-sections, average grain sizes within the trenches had large standard deviations, making it difficult to conclusively observe trends with variation in additive ratios. However, the percent grain area occupied by large grains (>200 nm) in the 250 nm and 500 nm wide trenches were much higher (65% and 77%, respectively) for the Cu deposited without organic additives than for depositions that included organics in the bath (typically <50%). Smaller Cu grain sizes have been found in previous studies[11,22] from the use of these organic additives, as they can disrupt atomic arrangement during deposition or create defects in the structure, that may impede grain growth by

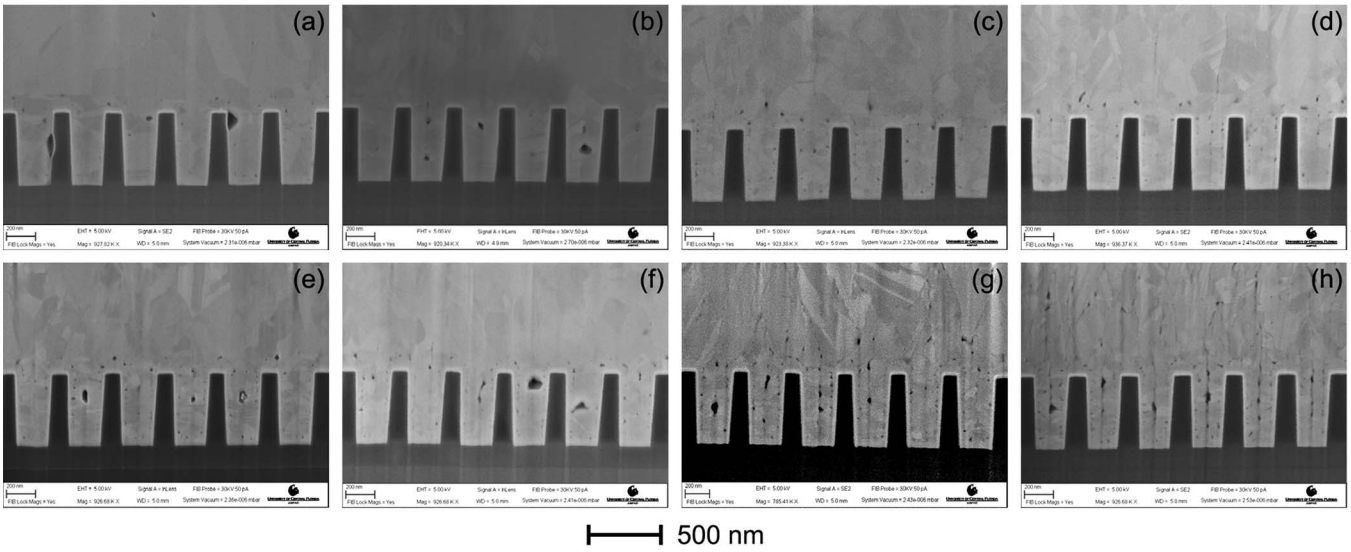

Figure 3. The cross-sectional SEM micrographs show the amount of voids that formed in the 2.78 aspect ratio trenches deposited without organic additives (a) and with 200 mg/L of PEG and JGB/SPS ratios of 0 (b), 0.2 (c), 0.5 (d), 1 (e), 2 (f), 10 (g), and 20 (h).

pinning grain boundaries during recrystallization. While these smaller grains would influence the microscopic scale stresses in the Cu, the void-induced stress relaxation observed in Roughness and residual stress of the Cu section is on the global scale. Moreover, it appeared that the larger trenches were less geometrically constrained by the sidewalls. This allowed the grains to grow much larger as evident when comparing the >200 nm grain area% between the 500 nm and 250 nm trenches for all organic additive concentrations in Table II.

Texture in the trenches.—Orientations of the Cu microstructure were observed with EBSD and TKD inverse pole figure (IPF) maps, which assign a color to each grain's crystallographic orientation. The IPF maps for the 250 nm and 500 nm wide trenches are shown in Figure 4. Both trench sizes have similar microstructural orientations. The base of the trenches contains large (111) oriented Cu grains normal to the sample surface, while smaller, more randomly oriented, grains were found at the top of the trench cross-sections. These highly oriented grains were epitaxial to the Cu seed layer orientations, as evident from rocking curve measurements conducted on the pre-deposited samples. A XRD rocking curve was performed on the seed layer by rotating the sample along the chi angle (rotation about the axis of the incident beam) at the 2θ of the (111) peak. Figure 5 shows the rocking curve and its apparent peak intensity around 0° chi, which indicates a large volume of (111) oriented grains normal to the Cu seed layer surface. The (111) peak at ∼43.2668° was, also, the only Cu peak found in the XRD 2θ scan of the seed layer, giving further evidence of a preferentially oriented seed layer.

A closer inspection of the inverse pole figure (IPF) maps revealed the grains at the top of the trenches may be textured. Figure 6 shows the IPF maps in the normal, transverse, and longitudinal directions of the 250 nm trenches deposited with and without organic additives. Grains grown from the sidewalls of the trenches appeared to be (111) textured in the transverse direction as opposed to the normal direction. This is especially apparent in the Cu deposited with organic additives and further exemplifies the (111) Cu seed layer orientation normal to its surface.

The introduction of organic additives into the electrodeposition bath resulted in base grain impingement and a higher likelihood that the grains would mimic the sidewall seed layer orientations. The reduction in overall texture within the trenches is evident from the lower (111) multiples of uniform density (MUD) shown in Table III. The MUD is a quantitative analysis of a microstructure's texture. A MUD higher than unity represents a textured microstructure, with increasing values indicating larger degrees of preferential orientation. The MUD data indicates highly preferential Cu (111) orientation in the normal direction for all bath chemistries used for deposition. The MUD of the 500 nm wide trenches were typically much larger than their 250 nm counterparts. From the IPF maps in Figure 4, this appears to be the result of larger base (111) grains in the trenches. Since the 500 nm trenches are not as constrained by the sidewalls, the base grains are allowed to grow further and occupy more area within the trenches.

Texture coefficient measurements, shown in Figure 7, confirmed the highest degree of preferential (111) oriented microstructures occurred without the use of organic additives; however, it also showed a different trend with the concentration of the organic additives. Similar to the roughness and stress measurements, the (111) texture coefficient decreased with increasing JGB/SPS ratio. Even at the highest JGB/SPS ratio (20) used in the bath, the (111) texture coefficient still appeared high, never falling below 3.95 out of 4.00 across the range

Table II. The Cu grain size comparisons between the two trench sizes and additive chemistries used for deposition.

		250 nm Trenches		500 nm Trenches	
PEG/SPS/JGB (mg/L)	JGB/SPS Ratio	Average Grain Diameter (nm)	>200 nm Grain Area%	Average Grain Diameter (nm)	>200 nm Grain Area%
0/0/0	N/A	123 ± 92	65%	197 ± 125	77%
200/20/10	0.5	110 ± 55	27%	121 ± 65	35%
200/5/10	2	111 ± 45	23%	112 ± 81	61%
200/5/100	20	121 ± 61	38%	155 ± 66	50%

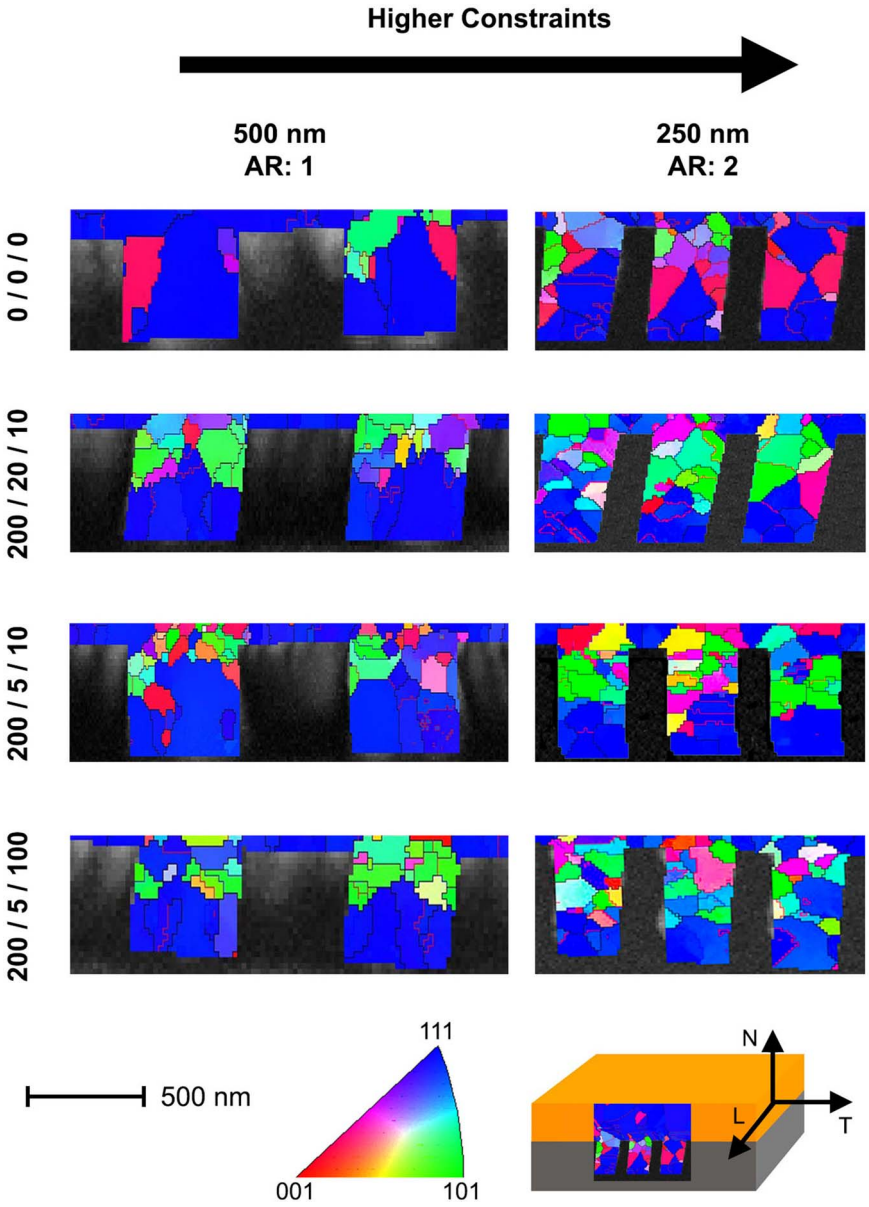

Figure 4. The inverse pole figure maps are shown for the 250 nm and 500 nm trench cross-sections and for each organic additive combination studied.

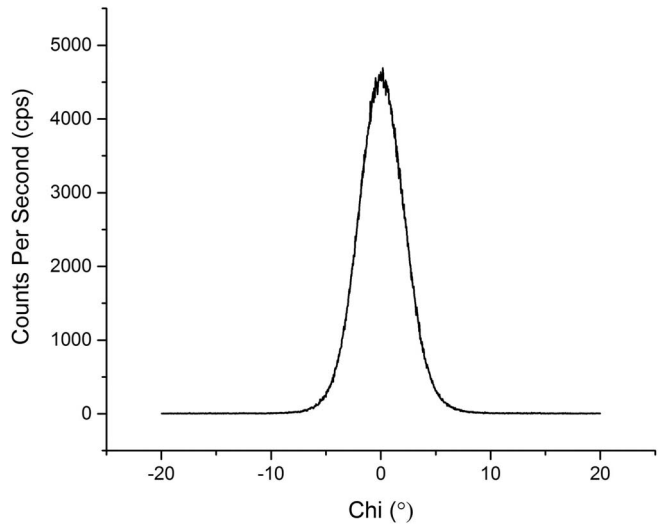

Figure 5. The XRD rocking curve of the trench seed layer.

tested. Variations between the XRD data and electron diffraction techniques is expected, since EBSD and TKD are a snap shot on a very small scale, while the XRD spot size encompasses almost the entire sample dimensions (20 mm × 20 mm).

The microstructural orientation in Cu has been shown to vary due to different mechanisms for grain growth;[36,37] however, it is unlikely that the same growth mechanism is responsible for all the variations seen in this study. It appears the Cu orientation inside the trenches was significantly dictated by the seed layer and impingement from organic additives. This suggests that the driving mechanism for variations in the Cu orientation in this study is the organic additive's ability to disrupt atomic stacking of Cu during deposition.

Strain and twin density.—Strain component maps were also obtained from the EBSD and TKD and are shown in Figure 8. Strain was estimated by comparing the local misorientation within a grain to the average misorientation across the entire grain. Areas of high strain concentrations are shown in red and appeared to be localized inside the trenches of the 0/0/0 deposited Cu. This is apparent in the 250 nm trenches due to their higher geometric constraint (larger aspect ratio) than the 500 nm wide trenches. Earlier results, *vide supra*, showed

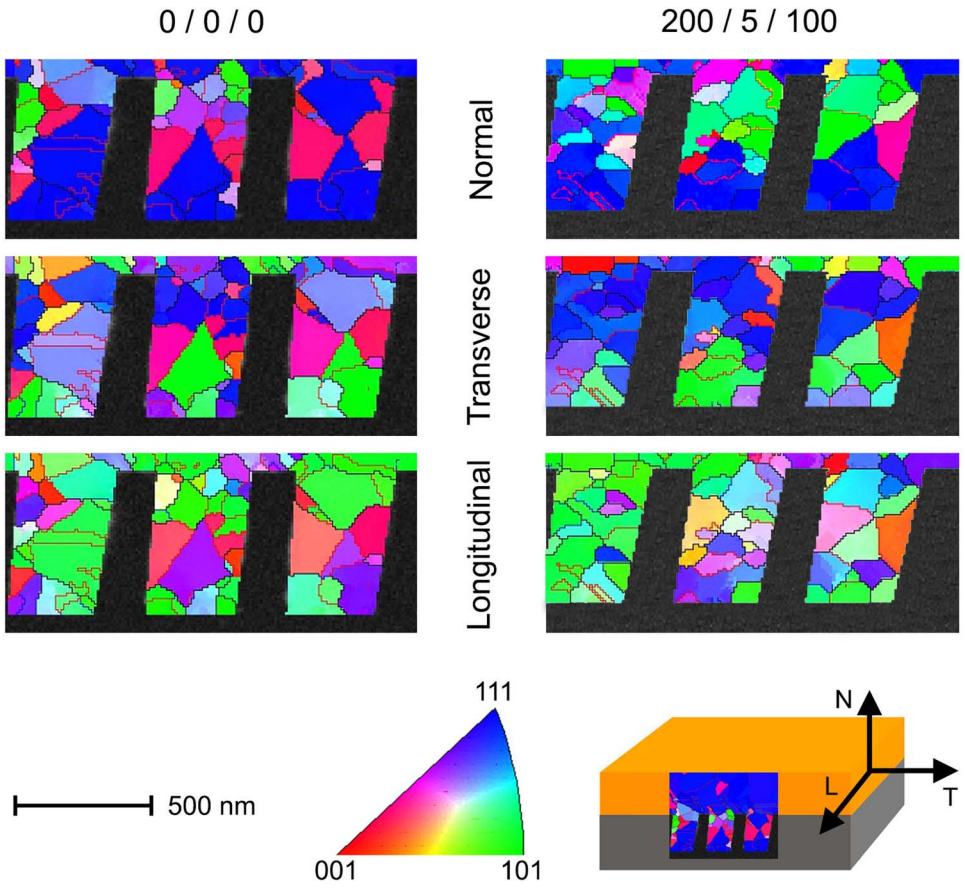

Figure 6. The cross-sectional inverse pole figure maps in the normal, transverse, and longitudinal directions for the 250 nm wide trenches deposited with and without organic additives.

that the increased void area in the trenches minimized the stresses found in the Cu. These voids explain the lower strains observed in the 200/20/10 trenches in Figure 8. Instead, high strain concentrations were found in areas of small grain clusters, where there are large volumes of grain boundaries. Higher strains in these areas could be a result of dislocation pile up at the high angle boundaries[38] or from the elastic anisotropy of Cu. Since grain orientations have different elastic constants,[39] strains can build up at locations where grains meet (triple junctions, grain boundaries, etc.).

Twin density was measured by counting the number of twins per unit area in the Cu trenches. The twin densities for the 250 nm and 500 nm wide trenches are listed in Table IV. As expected, the twin densities generally followed the same trends as the stress/strain measurements. The large strain concentrations in the 250 nm trenches created more twins than the 500 nm trenches. The 250 nm trenches filled without organic additives had more twins than those filled with organics due to the expected lower void area and higher stresses. However, the 500 nm trenches had larger twin densities when organics were utilized in the bath chemistry. This could be a result of less void content, since the trenches have a lower aspect ratio and should have been less prone to filling voids. Furthermore, the organic molecules may have disrupted the lattice formation during deposition and resulted in more twins.

Table III. The multiples of uniform density of the cross-sectional 250 nm and 500 nm wide trench microstructures of the Cu deposited with different organic additive concentrations.

	Multiple of Uniform Density (MUD)	
PEG/SPS/JGB (mg/L)	250 nm Trenches	500 nm Trenches
0 / 0 / 0	25 ± 5	30 ± 1
200 / 20 / 10	10 ± 2	23 ± 3
200 / 5 / 10	15 ± 3	14 ± 2
200 / 5 / 100	6 ± N/A	20 ± 2

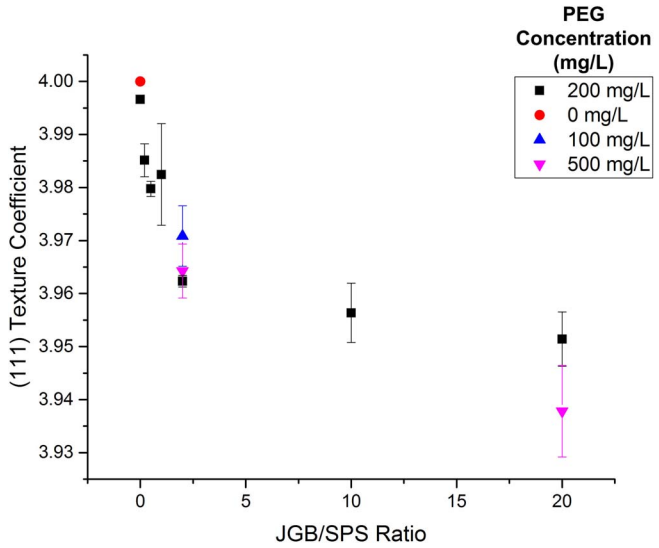

Figure 7. The change in (111) texture coefficient of Cu with JGB/SPS ratio in the electrodeposition bath.

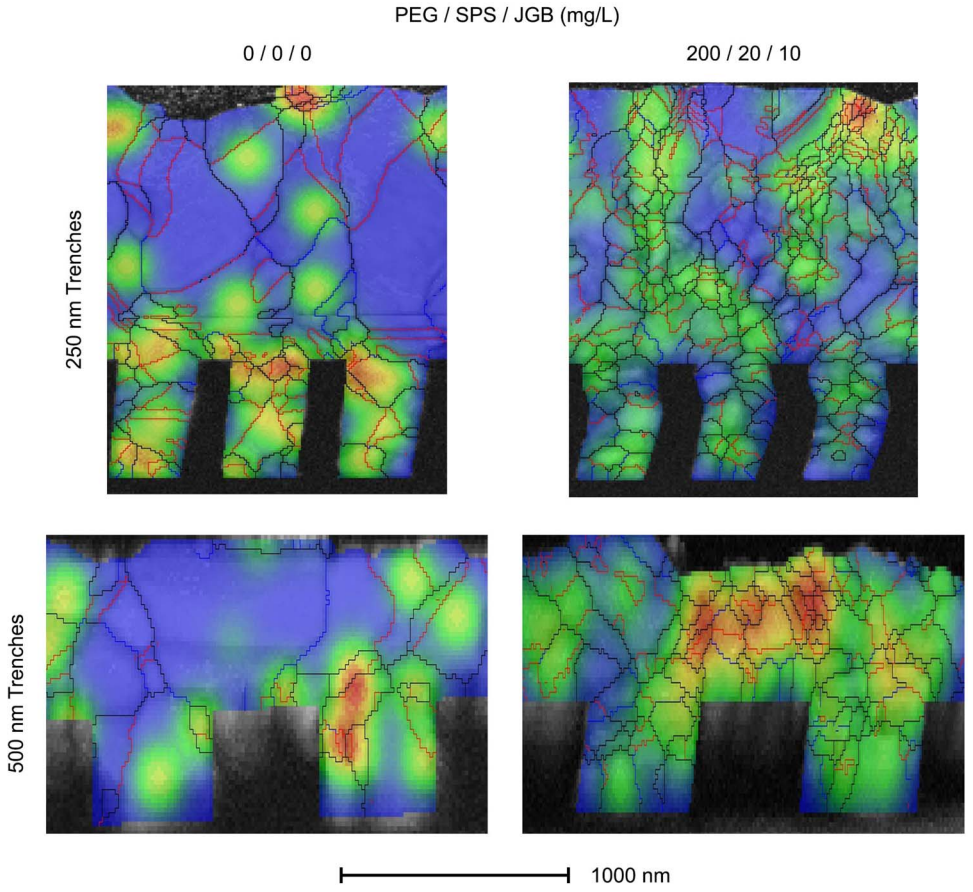

Figure 8. The strain components maps for the 250 nm and 500 nm wide trench cross-sections deposited with and without organic additives in the bath. All observed stresses were tensile in nature, with areas larger strain indicated by red and smaller strains shown in blue.

Table IV. The twin density of the Cu microstructure with trench size and organic additive concentrations used during deposition.

	Twins/μm^2	
PEG/SPS/JGB (mg/L)	250 nm Trenches	500 nm Trenches
0 / 0 / 0	40	11
200 / 20 / 10	33	32
200 / 5 / 10	35	23
200 / 5 / 100	21	17

Conclusions

The cross-sectional microstructures of two different aspect ratio trenches were evaluated with variation in the organic additive concentrations used in the electrodeposition bath. The leveler to accelerator (JGB/SPS) ratio appeared to significantly influence the properties of the Cu, while the PEG concentration had minimal impact. The residual biaxial stresses, measured by wafer curvature, decreased with increasing JGB/SPS ratio due to the larger void presence within the trenches. Grain sizes decreased with the introduction of the organic additives in the bath from impingement and resulted in smaller surface RMS roughness of the Cu. The adsorption of chemical additives into the Cu appears to have a more significant impact on the cross-sectional microstructure in this study than found, previously, on Cu surface microstructures. The texture within the trenches was found to be (111) preferentially oriented; however, the degree of preferential orientation decreased when organics were used by allowing the side-wall seed layer orientation to dictate more of the Cu orientations in the trenches.

Since the texture of the electroplated Cu was epitaxial to the seed layer orientation, it is reasonable to suggest that the Cu seed layer only be deposited onto the base of the trenches. However, more work is needed to conclusively state whether deposition purely onto a base seed layer would result in larger overall grain sizes and more highly textured trenches. Lastly, more geometrically constrained trenches were found to produce higher twin densities. These twin densities were lower in trenches that were filled with organic additives, since voids acted as the stress relieving mechanism in these trenches.

Acknowledgments

A contribution from U.S. National Institute of Standards and Technology, not subject to copyright. All views expressed in this paper are those of the authors and of others whom attribution is given and are not necessarily those of NIST nor of any of the institutions cited therein. The authors thank the Research Triangle Nanotechnology Network (grant no. 570508) and the National Institute of Standards and Technology (grant no. 60NANB12H016N) for their financial support. The assistance of the North Carolina State University's Analytical Instrumentation Facility and Roberto Garcia are also greatly appreciated as they provided assistance with the microscopy. Furthermore, the authors greatly appreciate the microscopy and XRD support from the University of Central Florida's Materials Characterization Facility and Dr. Taghi Darroudi at Clemson University's Electron Microscopy Laboratory. The authors would also like to thank Amrita Kapat for assisting with the roughness and wafer curvature measurements.

References

1. A. Pratt, Overview of the Use of Copper Interconnects in the Semiconductor Industry, Adv Energy Ind (2004).
2. J. Marro, C. Okoro, Y. Obeng, and K. Richardson, Defect and microstructural evolution in thermally cycled Cu through-silicon vias, *Microelectronics Reliability*, **54**, 2586 (2014).
3. A. S. Budiman, H. A. S. Shin, B. J. Kim, S. H. Hwang, H. Y. Son, M. S. Suh, Q. H. Chung, K. Y. Byun, N. Tamura, M. Kunz, and Y. C. Joo, "Measurement of stresses in Cu and Si around through-silicon via by synchrotron X-ray microdiffraction for 3-dimensional integrated circuits," *Microelectronics Reliability*, **52**, 530 (2012).
4. C. Okoro, J. W. Lau, F. Golshany, K. Hummler, and Y. S. Obeng, "A Detailed Failure Analysis Examination of the Effect of Thermal Cycling on Cu TSV Reliability," *Electron Devices, IEEE Transactions on*, **61**, 15 (2014).
5. J. A. Nucci, R. R. Keller, J. E. Sanchez, and Y. Shacham-Diamand, "Local crystallographic texture and voiding in passivated copper interconnects," *Appl. Phys. Lett.*, **69**, 4017 (1996).
6. O. Anderoglu, A. Misra, F. Ronning, H. Wang, and X. Zhang, "Significant enhancement of the strength-to-resistivity ratio by nanotwins in epitaxial Cu films," *J. Appl. Phys.*, **106**, 024313; 024313 (2009).
7. L. Lu, X. Chen, X. Huang, and K. Lu, "Revealing the Maximum Strength in Nanotwinned Copper," *Science*, **323**, 607 (2009).
8. C. Ryu, K. Kwon, A. L. Loke, H. Lee, T. Nogami, V. M. Dubin, R. A. Kavari, G. W. Ray, and S. S. Wong, "Microstructure and reliability of copper interconnects," *Electron Devices, IEEE Transactions on*, **46**, 1113 (1999).
9. X. Zhang and A. Misra, "Superior thermal stability of coherent twin boundaries in nanotwinned metals," *Scr. Mater.*, **66**, 860 (2012).
10. L. Vanasupa, Y. Joo, P. R. Besser, and S. Pramanick, "Texture analysis of damascene-fabricated Cu lines by X-ray diffraction and electron backscatter diffraction and its impact on electromigration performance," *J. Appl. Phys.*, **85**, 2583 (1999).
11. J. Neuner, I. Zienert, A. Peeva, A. Preuße, P. Kücher, and J. W. Bartha, "Microstructure in copper interconnects–Influence of plating additive concentration," *Microelectronic Engineering*, **87**, 254 (2010).
12. K. Ganesh, A. Darbal, S. Rajasekhara, G. Rohrer, K. Barmak, and P. Ferreira, "Effect of downscaling nano-copper interconnects on the microstructure revealed by high resolution TEM-orientation-mapping," *Nanotechnology*, **23**, 135702 (2012).
13. C. Okoro, R. Labie, K. Vanstreels, A. Franquet, M. Gonzalez, B. Vandevelde, E. Beyne, D. Vandepitte, and B. Verlinden, "Impact of the electrodeposition chemistry used for TSV filling on the microstructural and thermo-mechanical response of Cu," *Journal of Materials Science*, **46**, 3868 (2011).
14. H. Shin, B. Kim, J. Kim, S. Hwang, A. Budiman, H. Son, K. Byun, N. Tamura, M. Kunz, D. Kim, and Y. Joo, "Microstructure Evolution and Defect Formation in Cu Through-Silicon Vias (TSVs) During Thermal Annealing," *Journal of Electronic Materials*, **41**, 712 (2012).
15. C. Okoro, P. Kabos, J. Obrzut, K. Hummler, and Y. S. Obeng, "Accelerated Stress Test Assessment of Through-Silicon Via Using RF Signals, Electron Devices," *IEEE Transactions on*, **60**, 2015 (2013).
16. T. Moffat, J. Bonevich, W. Huber, A. Stanishevsky, D. Kelly, G. Stafford, and D. Josell, "Superconformal electrodeposition of copper in 500nm features," *J. Electrochem. Soc.*, **147**, 4524 (2000).
17. J. Tang, Q. Zhu, Y. Zhang, X. Zhang, J. Guo, and J. Shang, "Copper Bottom-up Filling for Through Silicon Via (TSV) Using Single JGB Additive," *ECS Electrochemistry Letters*, **4**, D28 (2015).
18. M. Hasegawa, Y. Negishi, T. Nakanishi, and T. Osaka, "Effects of additives on copper electrodeposition in submicrometer trenches," *J. Electrochem. Soc.*, **152**, C221 (2005).
19. P. M. Vereecken, R. A. Binstead, H. Deligianni, and P. C. Andricacos, "The chemistry of additives in damascene copper plating," *IBM Journal of Research and Development*, **49**, 3 (2005).
20. T. P. Moffat, D. Wheeler, W. H. Huber, and D. Josell, "Superconformal Electrodeposition of Copper," *Electrochemical and Solid-State Letters*, **4**, C26 (2001).
21. T. P. Moffat, D. Wheeler, and D. Josell, "Electrodeposition of Copper in the SPS-PEG-Cl Additive System: I. Kinetic Measurements: Influence of SPS," *Journal of The Electrochemical Society*, **151**, C262 (2004).
22. J. J. Kelly, C. Tian, and A. C. West, "Leveling and Microstructural Effects of Additives for Copper Electrodeposition," *Journal of The Electrochemical Society*, **146**, 2540 (1999).
23. G. Fabricius, K. Kontturi, and G. Sundholm, "Influence of thiourea on the nucleation of copper from acid sulfate solutions," *Electrochim. Acta*, **39**, 2353 (1994).
24. H. Natter and R. Hempelmann, "Nanocrystalline Copper by Pulsed Electrodeposition: The Effects of Organic Additives, Bath Temperature, and pH," *J. Phys. Chem.*, **100**, 19525 (1996).
25. R. Manu and S. Jayakrishnan, "Influence of polymer additive molecular weight on surface and microstructural characteristics of electrodeposited copper," *Bull. Mater. Sci.*, **34**, 347 (2011).
26. J. Marro, Tunable Copper Microstructures in Blanket Films and Trenches Using Pulsed Electrodeposition, ProQuest Dissertations and Theses (2016).
27. J. Marro, T. Darroudi, C. Okoro, Y. Obeng, and K. Richardson, "The Influence of Pulsed Electroplating Frequency and Duty Cycle on Copper Film Microstructure and Stress State," *Thin Solid Films*, **621**, 91 (2017).
28. W. Wu, S. Brongersma, M. Van Hove, and K. Maex, "Influence of surface and grain-boundary scattering on the resistivity of copper in reduced dimensions," *Appl. Phys. Lett.*, **84**, 2838 (2004).
29. Z. Choi, R. Mönig, and C. V. Thompson, "Dependence of the electromigration flux on the crystallographic orientations of different grains in polycrystalline copper interconnects," *Appl. Phys. Lett.*, **90**, (2007).
30. S. Kang, Y. Obeng, M. Decker, M. Oh, S. Merchant, S. Karthikeyan, C. Seet, and A. Oates, "Effect of annealing on the surface microstructural evolution and the electromigration reliability of electroplated Cu films," *J Electron Mater*, **30**, 1506 (2001).
31. R. Huang, W. Robl, H. Ceric, T. Detzel, and G. Dehm, "Stress, Sheet Resistance, and Microstructure Evolution of Electroplated Cu Films During Self-Annealing, Device and Materials Reliability," *IEEE Transactions on*, **10**, 47 (2010).
32. G. G. Stoney, "The tension of metallic films deposited by electrolysis, Proceedings of the Royal Society of London. Series A," *Containing Papers of a Mathematical and Physical Character*, **82**, 172 (1909).
33. R. R. Keller and R. H. Geiss, "Transmission EBSD from 10 nm domains in a scanning electron microscope," *J. Microsc.*, **245**, 245 (2012).
34. Keshra Sangwal, *Additives and crystallization processes: from fundamentals to applications*, John Wiley & Sons 2007.
35. L. W. Kong, J. R. Lloyd, K. B. Yeap, E. Zschech, A. Rudack, M. Liehr, and A. Diebold, "Applying X-ray microscopy and finite element modeling to identify the mechanism of stress-assisted void growth in through-silicon vias," *J. Appl. Phys.*, **110**(5), 053502 (2011).
36. C. V. Thompson, "Texture evolution during grain growth in polycrystalline films," *Scripta Metallurgica et Materialia*, **28**, 167 (1993).
37. E. M. Zielinski, R. P. Vinci, and J. C. Bravman, "Effects of barrier layer and annealing on abnormal grain growth in copper thin films," *J. Appl. Phys.*, **76**, 4516 (1994).
38. R. E. Smallman and A. Ngan, *Physical metallurgy and advanced materials*, Butterworth-Heinemann 2011.
39. G. Simmons and H. Wang, Single crystal elastic constants and calculated aggregate properties, (1971).